Analysis of Chromatic Dispersion-Induced Second-Harmonic Distortions Including Laser Dynamics to the Second Order

Ki-Hyuk Lee, Hyun-Yong Choi, and Woo-Young Choi, *Member, IEEE*

***Abstract*—We perform analysis of chromatic dispersion-induced second-harmonic distortions including laser diode dynamics. Investigating laser diode dynamics fully to the second order, we derive analytical expressions for intensity and frequency modulation indices. Using these, we accurately model chromatic dispersion-induced second-harmonic distortions for signals produced by a directly modulated distributed feedback laser. The results agree well with numerical solutions, as well as with experimental results for a wide range of modulation frequencies and fiber lengths.**

***Index Terms*—Chromatic dispersion, laser diode dynamics, second-harmonic distortion, semiconductor laser diode.**

I. Introduction

THERE is a strong need for analog optical communication systems [1]–[3]. The CATV and radio-on-fiber system are examples in which high frequency carriers and subcarrier multiplexed data are simultaneously transmitted over the fiber. In these systems, one of the key elements that determine the total system performance is optical source linearity. Direct modulation of semiconductor laser diodes is the simplest and most economical solution, but linearity of the laser diode is often not sufficient for many applications. Consequently, it is of significant importance to understand the causes for nonlinearity in laser diodes and consequent performance degradation in analog optical links.

When laser diodes are directly modulated, there are several causes for nonlinearity. In subcarrier multiplexed systems, which usually have many channels in the range of a few hundred megahertz, static nonlinear resistance–capacitance (*L–I*) characteristics and clipping can be the main causes for distortion [4]. Laser diode chirp also causes signal distortions when modulated optical signals are transmitted through the dispersive medium [5], [6]. In addition, laser diodes have intrinsic dynamic nonlinearity, which by itself and with the combination of fiber dispersion causes distortions [7], [8]. The nonlinearity that we are interested in is this dynamic nonlinearity.

In order to understand the influence of dynamic nonlinearity of a laser diode, the E-field of laser diode output, when the laser diode is directly modulated by the sinusoidal current with angular frequency ω, can be modeled as [9]

$$E(t,z=0) \cong P_0^{\frac{1}{2}} \left(1+\sum_{n=1}^{\infty} m_{IMn}\cos(n\omega\cdot t+\varphi_{IMn})\right)^{\frac{1}{2}} \cdot \exp\left(j\cdot\sum_{n=1}^{\infty} m_{\mathrm{FMn}}\sin(n\omega\cdot t+\varphi_{\mathrm{FMn}})\right). \quad (1)$$

The above model includes all the possible harmonic terms in magnitude and phase, each of which has intensity modulation (IM) index $\mathrm{m_{IMn}}$, and frequency modulation (FM) index $\mathrm{m_{FMn}}$. The higher order harmonic terms are produced by the dynamic nonlinearity of the laser diode. Since each harmonic term does not necessarily have the same phase value, φ_{IMn} and φ_{FMn} are used to represent their values.

For the simplest possible analysis, the influence of all the higher order harmonics can be ignored [5], [6] and the E-field can be simply modeled as

$$E(t,z=0) \cong P_0^{\frac{1}{2}} \left(1+m_{\mathrm{IM1}}\cos(\omega\cdot t+\varphi_{\mathrm{IM1}})\right)^{\frac{1}{2}} \cdot \exp\left(j\cdot m_{\mathrm{FM1}}\sin(\omega\cdot t+\varphi_{\mathrm{FM1}})\right). \quad (2)$$

In the above model, the effect of laser chirp is included by $\mathrm{m_{FM1}}$. Using this field model, Meslener [5] analytically showed that the combination of the first-order FM, or laser chirp, combined with the fiber dispersion causes harmonic distortions when signals are photodetected after transmission in the fiber. But, as will be shown in this paper, this approach has insufficient accuracy because the directly modulated laser diode dynamics provide another source of nonlinearity, in addition to the distortion induced by chirp and chromatic dispersion.

For a more accurate model, Kuo [7] and Lin [8] included the second-order IM effect and achieved better accuracy in predicting the second-harmonic distortions for CATV applications. This model can be represented as

$$E(t,z=0) \cong P_0^{\frac{1}{2}} \left(1+m_{\mathrm{IM1}}\cos(\omega\cdot t+\varphi_{\mathrm{IM1}}) +m_{\mathrm{IM2}}\cos(2\omega\cdot t+\varphi_{\mathrm{IM2}})\right)^{\frac{1}{2}} \cdot \exp\left(j\cdot m_{\mathrm{FM1}}\sin(\omega\cdot t+\varphi_{\mathrm{FM1}})\right). \quad (3)$$

We find that this model is not sufficiently accurate when the modulation frequency increases. For better accuracy, we include the second-order FM effect. In addition, we specifically consider the phase difference between each IM and FM harmonic term, or $\varphi_{\mathrm{IM2}}-\varphi_{\mathrm{IM1}}$ and $\varphi_{\mathrm{FM2}}-\varphi_{\mathrm{IM1}}$, which have been ne-

Manuscript received July 26, 2002; revised November 19, 2002. This work was supported by the Ministry of Science and Technology of Korea through the National Research Laboratory program.

The authors are with the Department of Electrical and Electronic Engineering, Yonsei University, Seoul 120-749, Korea (e-mail: wchoi@yonsei.ac.kr).

Digital Object Identifier 10.1109/JQE.2003.810273

glected in previous studies. With this, the E-field model used in our investigation becomes

$$E(t,z=0) \cong P_0^{\frac{1}{2}} \left(1+m_{\mathrm{IM1}}\cos(\omega\cdot t+\varphi_{\mathrm{IM1}}) +m_{\mathrm{IM2}}\cos(2\omega\cdot t+\varphi_{\mathrm{IM2}})\right)^{\frac{1}{2}} \cdot \exp\left(j\cdot m_{\mathrm{FM1}}\sin(\omega\cdot t+\varphi_{\mathrm{FM1}}) +j\cdot m_{\mathrm{FM2}}\sin(2\omega\cdot t+\varphi_{\mathrm{FM2}})\right). \quad (4)$$

For our analysis, we first derive analytical expressions for all the parameters appearing in the above model using the perturbation approach based on the rate equations. In addition, we consider the influence of fiber dispersion on the second-harmonic distortions when signals are detected after traveling over the fiber. To confirm the accuracy of the analytical procedure, we perform full numerical analyses of the laser rate equations, as well as experimental verification in a wide range of modulation frequencies and transmission distances.

This paper is organized as following. In Section II, the nonlinear dynamics of laser diode is analyzed and modulation index parameters are determined. In Section III, dispersion-induced second-harmonic distortions are derived and these are compared with the results obtained from full numerical solutions. In Section IV, comparisons are made with the results of experimental verification. Then, in Section V, the paper is concluded.

II. Nonlinear Dynamics of Laser Diode

The first task is determining analytical expressions for modulation indices and phase terms in the E-field model given by (4). For this, we used the perturbation approach based on laser rate equations [10], [11]. The rate equations used in our analysis are modified rate equations given as [12]

$$\begin{aligned}
\frac{dP(t)}{dt} &= \frac{B\tau_n I_{\mathrm{th}}\left(X(t)-1\right)+\frac{1}{\tau_p}}{1+\mathrm{FB}\tau_p\tau_c P(t)}P(t)-\frac{P(t)}{\tau_p}\\
\frac{dX(t)}{dt} &= \frac{I(t)}{I_{\mathrm{th}}\tau_n}-\frac{\mathrm{FB}\tau_p\left(X(t)-1\right)+\frac{F}{I_{\mathrm{th}}\tau_n}}{1+\mathrm{FB}\tau_p\tau_c P(t)}P(t)-\frac{X(t)}{\tau_n}\\
\Delta\nu(t) &= \frac{1}{2\pi}\frac{d\phi(t)}{dt}=\frac{1}{2\pi}\frac{\alpha}{2}B\tau_n I_{\mathrm{th}}\left(X(t)-1\right)
\end{aligned} \quad (5)$$

where $P(t)$ is the output optical power, X(t) is the normalized carrier density, and ϕ(t) is the phase of optical field. B and F are combinations of several parameters: $B=\Gamma g_0/qV$ where Γ is the confinement factor, g_0 is gain slope, q is the electron charge, V is the volume of the active region, and $F=2q\lambda/hc\eta$, where λ is the wavelength, h is the Plank constant, c is the speed of light, and η is the quantum efficiency. In addition, I_{th} is the threshold current, I_s is the spontaneous emission current, τ_p is the photon lifetime, τ_n is the carrier lifetime, and $\tau_c=\varepsilon/g_0$, where ε is the gain compression factor and α is the linewidth-enhancement factor. This particular set of rate equations is used in our investigation since it is most suitable for experimentally extracting numerical values for the rate equation parameters, thus making it possible to compare analytical and experimental results. Rate equation parameters were extracted following the procedure given in [12] for a commercially available butterfly-type packaged DFB laser, and the results are summarized in Table I.

For the nonlinear distortion analysis, we used the standard perturbation method in which a sinusoidal input current of small magnitude with modulation frequency ω is assumed, or $I(t)=I_0+(1/2)(\Delta I_1 e^{j\omega t}+\Delta I_1^* e^{-j\omega t})$. Then, the resulting responses for the optical power, normalized carrier density, and lasing frequency shift can be expressed as follows:

$$\begin{aligned}
P(t) &= P_0+\frac{1}{2}(\Delta P_1 e^{j\omega t}+\Delta P_1^* e^{-j\omega t}) +\frac{1}{2}(\Delta P_2 e^{j2\omega t}+\Delta P_2^* e^{-j2\omega t})+\cdots\\
X(t) &= X_0+\frac{1}{2}(\Delta X_1 e^{j\omega t}+\Delta X_1^* e^{-j\omega t}) +\frac{1}{2}(\Delta X_2 e^{j2\omega t}+\Delta X_2^* e^{-j2\omega t})+\cdots\\
\Delta\nu(t) &= \upsilon_0+\frac{1}{2}(\Delta\nu_1 e^{j\omega t}+\Delta\nu_1^* e^{-j\omega t}) +\frac{1}{2}(\Delta\nu_2 e^{j2\omega t}+\Delta\nu_2^* e^{-j2\omega t})+\cdots.
\end{aligned} \quad (6)$$

Inserting the above equations into the rate equations, we can derive relationships for the first-order terms as in (7) and second-order terms in (9). In these equations, each coefficient is function of lower order terms and ω as shown in (8), (10), and (11)

$$\begin{aligned}
0 &= a_{11}\times\Delta P_1+a_{12}\times\Delta X_1\\
\Delta I_1 &= a_{21}\times\Delta P_1+a_{22}\times\Delta X_1\\
\Delta\nu_1 &= -a_{32}\times\Delta X_1
\end{aligned} \quad (7)$$

$$\begin{aligned}
a_{11} &= j\omega\cdot(1+\mathrm{FB}\tau_p\tau_c\cdot P_0)+B\tau_n I_{\mathrm{th}} +2\mathrm{FB}\tau_c\cdot P_0-B\tau_n I_{\mathrm{th}}(1-I_s\tau_p\tau_c)\cdot X_0\\
a_{12} &= -B\tau_n I_{\mathrm{th}}(1+I_s\tau_p\tau_c)\cdot P_0-\frac{I_s I_{\mathrm{th}}B\tau_n}{F}\\
a_{21} &= \frac{\left\{-\frac{\mathrm{FB}\tau_p\tau_c}{I_{\mathrm{th}}\tau_n}\cdot I_0-\mathrm{FB}\tau_p+\frac{F}{I_{\mathrm{th}}\tau_n}+\mathrm{FB}\tau_p\left(1+\frac{\tau_c}{\tau_n}\right)\cdot X_0\right\}}{\left(\frac{1}{I_{\mathrm{th}}\tau_n}+\frac{\mathrm{FB}\tau_p\tau_c}{I_{\mathrm{th}}\tau_n}\cdot P_0\right)}\\
a_{22} &= \frac{\left\{j\omega\cdot(1+\mathrm{FB}\tau_p\tau_c\cdot P_0)+\frac{1}{\tau_n}+\mathrm{FB}\tau_p\left(1+\frac{\tau_c}{\tau_n}\right)\cdot P_0\right\}}{\left(\frac{1}{I_{\mathrm{th}}\tau_n}+\frac{\mathrm{FB}\tau_p\tau_c}{I_{\mathrm{th}}\tau_n}\cdot P_0\right)}\\
a_{32} &= -\frac{1}{2\pi}\frac{\alpha}{2}B\tau_n I_{\mathrm{th}}
\end{aligned} \quad (8)$$

TABLE I
Extracted Values for for Laser - Diode Parameters

Parameters	Description	Dimension	Value
I_{th}	Threshold Current	mA	17.52
$F=2q\lambda/hc\eta$		A/W	12.56
I_s	Spontaneous emission term	μA	12.59
$B=\Gamma g_0/qV$		GHz^2/mA	176.34
K	K factor	ps	296.52
τ_n	Carrier Life Time	ns	0.179
α	Linewidth Enhancement Factor	-	3.09
$\tau_c=\varepsilon/g_0$		ps	3.18
τ_p	Photon Life Time	ps	4.33

and

$$\begin{aligned} K_1 &= b_{11} \times \Delta P_2 + b_{12} \times \Delta X_2 \\ K_2 &= b_{21} \times \Delta P_2 + b_{22} \times \Delta X_2 \\ \Delta\nu_2 &= -b_{32} \times \Delta X_2 \end{aligned} \tag{9}$$

$$\begin{aligned} b_{11} &= j2\omega \cdot (1 + \mathrm{FB}\tau_p\tau_c \cdot P_0) + B\tau_n I_{\mathrm{th}} \\ &\quad + 2\mathrm{FB}\tau_c \cdot P_0 - B\tau_n I_{\mathrm{th}}(1 + I_s\tau_p\tau_c) \cdot X_0 \\ b_{12} &= -\frac{I_s I_{\mathrm{th}} B\tau_n}{F} - B\tau_n I_{\mathrm{th}}(1 + I_s\tau_p\tau_c) \cdot P_0 \\ b_{21} &= -\frac{\mathrm{FB}\tau_p\tau_c}{I_{\mathrm{th}}\tau_n} \cdot I_0 - \mathrm{FB}\tau_p + \frac{F}{I_{\mathrm{th}}\tau_n} \\ &\quad + \mathrm{FB}\tau_p \left(1 + \frac{\tau_c}{\tau_n}\right) \cdot X_0 \\ b_{22} &= j2\omega \cdot (1 + \mathrm{FB}\tau_p\tau_c \cdot P_0) + \frac{1}{\tau_n} + \mathrm{FB}\tau_p \times \left(1 + \frac{\tau_c}{\tau_n}\right) \cdot P_0 \\ b_{32} &= -\frac{1}{2\pi}\frac{\alpha}{2} B\tau_n I_{\mathrm{th}} \end{aligned} \tag{10}$$

$$\begin{aligned} K_1 &= -\frac{\mathrm{FB}\tau_c}{2}(j\omega \cdot \tau_p + 1) \cdot \Delta P_1^2 + \frac{B\tau_n I_{\mathrm{th}}(1 + I_s\tau_p\tau_c)}{2} \\ &\quad \cdot \Delta X_1 \Delta P_1 \\ K_2 &= \frac{-\mathrm{FB}\tau_p}{2}\left(j\omega \cdot \tau_c + 1 + \frac{\tau_c}{\tau_n}\right) \cdot \Delta X_1 \Delta P_1 + \frac{\mathrm{FB}\tau_p\tau_c}{2I_{\mathrm{th}}\tau_n} \\ &\quad \cdot \Delta I_1 \Delta P_1. \end{aligned} \tag{11}$$

From the above equations, we can find the fundamental frequency components and second-harmonic distortion components as follows:

$$\Delta P_1 = \frac{-a_{12} \cdot \Delta I_1}{a_{11}a_{22} - a_{12}a_{21}}, \quad \Delta\nu_1 = \frac{-a_{32}a_{11} \cdot \Delta I_1}{a_{11}a_{22} - a_{12}a_{21}} \tag{12}$$

$$\Delta P_2 = \frac{K_1 b_{22} - K_2 b_{12}}{b_{11}b_{22} - b_{12}b_{21}}, \quad \Delta\nu_2 = \frac{-b_{32}(K_2 b_{11} - K_1 b_{21})}{b_{11}b_{22} - b_{12}b_{21}}. \tag{13}$$

Consequently, if ΔI_1 is known, expressions for all the parameters of interest can be found from the above equations. In addition, IM and FM indices and their phases can be defined as follows:

$$\begin{aligned} m_{\mathrm{Im1}} &= \frac{\Delta P_1}{P_0}, \; m_{\mathrm{Im2}} = \frac{\Delta P_2}{P_0}, \; \varphi_{\mathrm{Im1}} = \tan^{-1}\left(\frac{\mathrm{Im}(\Delta P_1)}{\mathrm{Re}(\Delta P_1)}\right) \\ \varphi_{\mathrm{Im2}} &= \tan^{-1}\left(\frac{\mathrm{Im}(\Delta P_2)}{\mathrm{Re}(\Delta P_2)}\right) \\ m_{\mathrm{FM1}} &= \frac{\Delta\nu_1}{f}, \; m_{\mathrm{FM2}} = \frac{\Delta\nu_2}{2f}, \; \varphi_{\mathrm{FM1}} = \tan^{-1}\left(\frac{\mathrm{Im}(\Delta\nu_1)}{\mathrm{Re}(\Delta\nu_1)}\right) \\ \varphi_{\mathrm{FM2}} &= \tan^{-1}\left(\frac{\mathrm{Im}(\Delta\nu_2)}{\mathrm{Re}(\Delta\nu_2)}\right) \end{aligned} \tag{14}$$

where Re{} and Im{} are used for expressing real and imaginary parts.

Fig. 1(a) shows the calculated first- and second-order IM indices, $\mathrm{m_{IM1}}$ and $\mathrm{m_{IM2}}$, Fig. 1(b) the FM indices, m_{FM1} and m_{FM2}, and Fig. 1(c) the values of phase terms in reference to φ_{IM1}. For the calculation, extracted values for the laser parameters given in Table I are used. The current modulation index $\Delta\mathrm{I_1}$ is set to 0.1 and the bias current at $1.9I_{\mathrm{th}}$. At this bias current, the relaxation resonance frequency is about 7.5 GHz. As

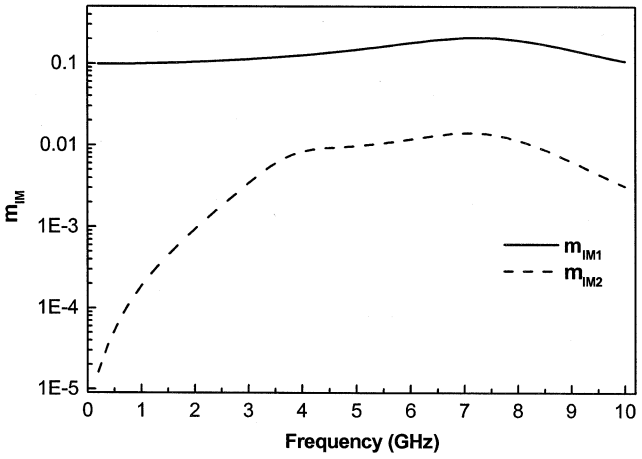

(a)

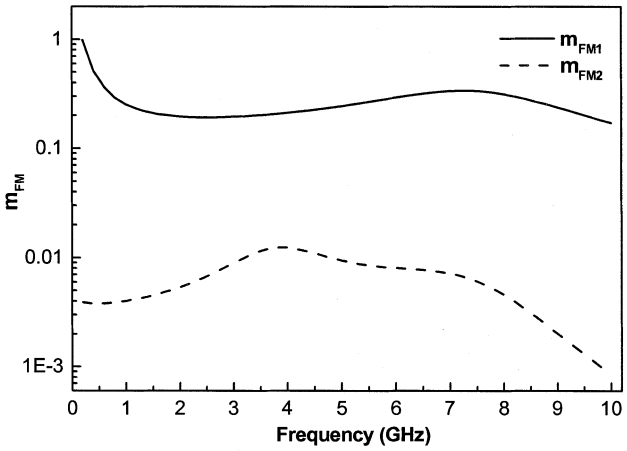

(b)

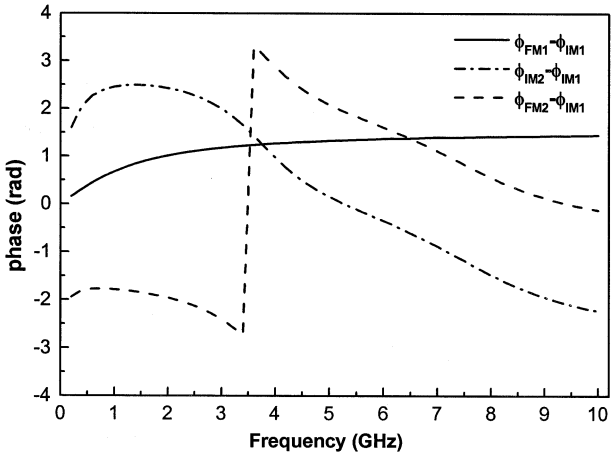

(c)

Fig. 1. Calculated modulation indices and phases. (a) IM index: $\mathrm{m_{IM1}}$ and $\mathrm{m_{IM2}}$. (b) FM index: $\mathrm{m_{FM1}}$ and $\mathrm{m_{FM2}}$. (c) Phase values in reference to φ_{IM1}.

can be seen, first-order IM and FM indices are enhanced at the resonance frequency. Because the first-order FM index is defined as $\Delta\nu_1/\mathrm{f}$, it becomes larger as the modulation frequency decreases. It is also observed that second-order intensity modulation indices m_{IM2} and m_{FM2} are enhanced in the range covering half the resonance frequency to the resonance frequency.

III. Influence of Fiber Dispersion on Distortions

The electric field of the laser output given in (4) can be expanded using Fourier series for intensity modulation components and frequency modulation components as follows:

$$E(t,z=0) \cong P_0^{\frac{1}{2}} \left(\sum_{n=-\infty}^{\infty} K_n \cdot e^{j\cdot n\cdot\omega\cdot t} \right) \cdot \left(\sum_{n=-\infty}^{\infty} J_n(m_{\mathrm{FM1}}) \cdot e^{j(n\cdot\omega\cdot t + n\cdot\varphi_{\mathrm{FM1}})} \right) \cdot \left(\sum_{n=-\infty}^{\infty} J_n(m_{\mathrm{FM2}}) \cdot e^{j(2\cdot n\cdot\omega\cdot t + n\cdot\varphi_{\mathrm{FM2}})} \right) \quad (15)$$

$$K_n = \int_T \frac{1}{T} \Big(1 + m_{\mathrm{IM1}} \cos(\omega\cdot t + \varphi_{\mathrm{IM1}}) + m_{\mathrm{IM2}} \cos(2\omega\cdot t + \varphi_{\mathrm{IM2}}) \Big)^{\frac{1}{2}} \cdot e^{j\cdot n\cdot\omega\cdot t} dt. \quad (16)$$

By collecting same frequency components, (15) becomes

$$E(t, z=0) \cong P_0^{\frac{1}{2}} \left(\sum_{n=-\infty}^{\infty} C_n \cdot e^{j\cdot n\cdot\omega\cdot t} \right)$$

where

$$C_n = \sum_{l=-\infty}^{\infty} J_l(m_{\mathrm{FM}_2}) e^{j\varphi_{\mathrm{FM2}}} \cdot \left(\sum_{k=-\infty}^{\infty} K_{-2l+n-k} \cdot J_k(m_{\mathrm{FM}_1}) e^{j\cdot k\cdot\varphi_{\mathrm{FM1}}} \right) \quad (17)$$

When such an electric field is propagated through fiber with the dispersion modeled as accrued quadratic phase, different harmonic components acquire different phase changes $e^{jn^2\theta}$, where $\theta = (\lambda^2 \cdot D \cdot L \cdot \omega^2)/(4\pi c)$ due to fiber dispersion [5].

At the receiver side, detected photocurrents are obtained by squaring the electric field magnitude. By expressing the phase of each harmonic field component as $\varphi_n = \tan^{-1}\{\mathrm{Im}(C_n)/\mathrm{Re}(C_n)\}$, the photocurrent becomes

$$\begin{aligned} I(t, z=L) &= |E(t, z=L)|^2 \\ &= \left(\sum_{n=-\infty}^{\infty} C_n e^{j(n\cdot\omega\cdot t + n^2\cdot\theta)} \right) \times \left(\sum_{n=-\infty}^{\infty} C_n e^{j(n\cdot\omega\cdot t + n^2\cdot\theta)} \right)^* \\ &= \left(\sum_{n=-\infty}^{\infty} |C_n| e^{j(n\cdot\omega\cdot t + n^2\cdot\theta + \varphi_n)} \right) \times \left(\sum_{n=-\infty}^{\infty} |C_n| e^{-j(n\cdot\omega\cdot t + n^2\cdot\theta + \varphi_n)} \right). \end{aligned} \quad (18)$$

After multiplying and gathering the same frequency components, the average detected current, the fundamental component, and the second-harmonic distortion become (19), (20), and (21), respectively

$$\mathrm{DC} = \sum_{n=-\infty}^{\infty} |C_n|^2 \quad (19)$$

$$\mathrm{F1}(\omega, L) = \left\{ \sum_{n=-\infty}^{\infty} |C_n||C_{n+1}| \cos((2\cdot n+1)\theta + \varphi_{n+1} - \varphi_n) \right\} \cdot \cos\omega t + \left\{ \sum_{n=-\infty}^{\infty} |C_n||C_{n+1}| \times \sin((2\cdot n+1)\theta + \varphi_{n+1} - \varphi_n) \times \sum_{n=-\infty}^{-1} -|C_n||C_{n+1}| \times \sin((2\cdot n+1)\theta + \varphi_{n+1} - \varphi_n) \right\} \sin\omega t \quad (20)$$

$$\mathrm{F2}(\omega, L) = \left\{ \sum_{n=-\infty}^{\infty} |C_n||C_{n+2}| \cos((4\cdot n+4)\theta + \varphi_{n+2} - \varphi_n) \right\} \cdot \cos 2\omega t + \left\{ \sum_{n=-\infty}^{\infty} |C_n||C_{n+2}| \times \sin((4\cdot n+4)\theta + \varphi_{n+2} - \varphi_n) + \sum_{n=-\infty}^{-1} -|C_n||C_{n+2}| \times \sin((4\cdot n+4)\theta + \varphi_{n+2} - \varphi_n) \right\} \cdot \sin 2\omega t. \quad (21)$$

Fig. 2 shows the resulting fundamental component, F1(ω, L) and the second-harmonic distortion, F2(ω, L) at various modulation frequencies and transmission distances. In the figure, solid lines represent the results obtained by using (20) and (21). In calculating these results, input current modulation index of 0.1 is used at the bias condition of $1.9\mathrm{I_{th}}$. For comparison, results obtained from previously reported models are shown in dashed [5], [6] and dashed-dotted lines [7], [8]. Dashed lines show the results when all the higher order effects are ignored or using the E-field model given in (2). Dashed-dotted lines show the results when distortions in frequency modulation are neglected, corresponding to the case of using the E-field given in (3). In addition, the results obtained from the full numerical solution of the rate equations are also shown for comparison. The Runge–Kutta method is used for numerically solving the rate equations using the parameter values given in Table I. The E-fields after traveling dispersive fiber are calculated by transforming the time-domain signal into the frequency domain, multiplying the fiber transfer function, and then transforming back to the time domain [8]. The photon-detected currents are obtained by squaring the magnitude of the resulting E-field. By calculating the power spectrum of the currents, the fundamental signal and the second-harmonic distortions are obtained. In the

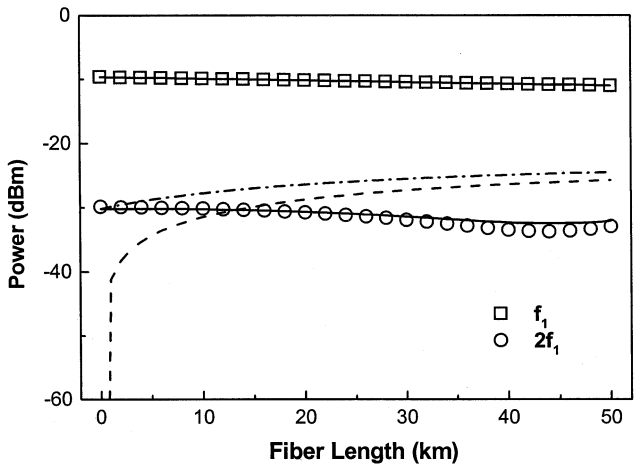

(a)

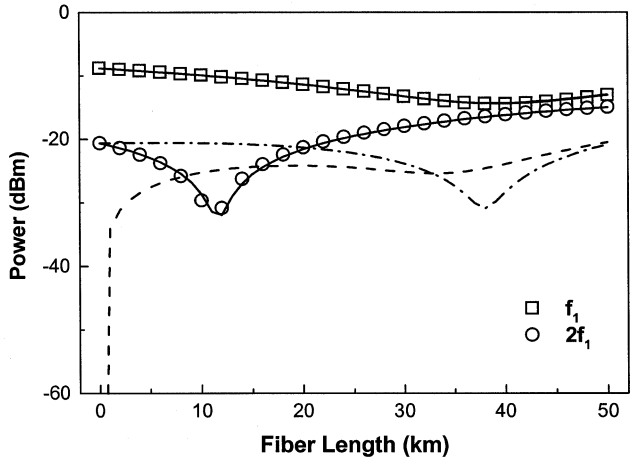

(b)

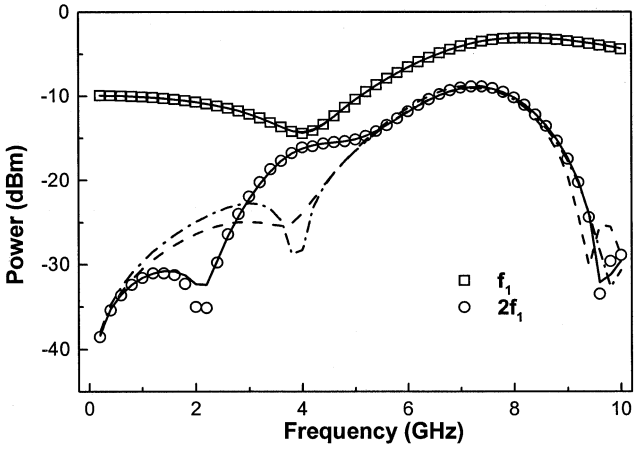

(c)

Fig. 2. Second-harmonic distortions obtained from exact numerical solutions (dots) and analyzes (lines) based on various models. (a) Fundamental signals and second-harmonic distortions at various fiber lengths for 2-GHz modulation. (b) Fundamental signals and second-harmonic distortions at various fiber lengths for 4-GHz modulation. (c) Fundamental signals and second-harmonic distortions at 40-km fiber for various modulation frequencies.

process, the fast Fourier transform (FFT) algorithm with a time step of 10^{-11} seconds and 10^4 sampling points is used. With this, the numerical solution is expected to provide exact results for the given parameters.

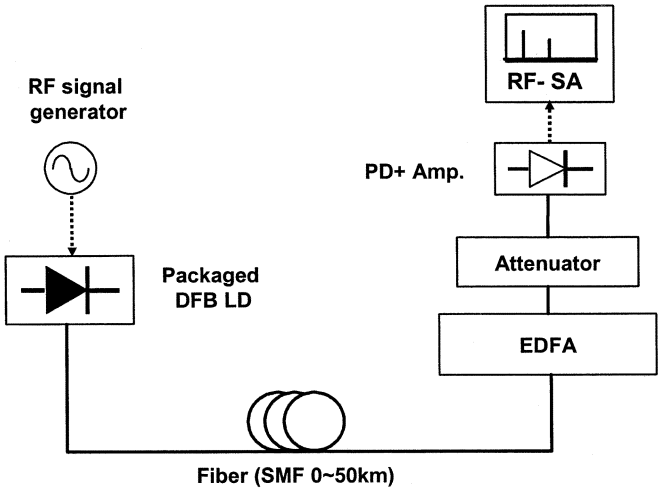

Fig. 3. Experimental setup.

As shown in Fig. 2(a) and (b), the E-field model of (2) does not provide reasonable answers for very short distances. This is because (2) ignores the intrinsic dynamic nonlinearity of the laser diode which is the main source of distortion at short distance, whereas the chirp-induced distortion in the wake of chromatic dispersion is negligible. Although E-field model of (3) shows good agreement in short distances, it shows disagreement as transmission length increases. As can be observed in Fig. 2(c), the accuracy of (2) and (3) is sufficiently good for very low or very high modulation frequency. At the low modulation frequency, the dynamic nonlinear effects are small and the first-order FM alone can explain the dispersion-induced second-harmonic distortions. At the high modulation frequency around the resonance frequency, the first-order FM becomes dominant again as can be seen from the enhanced $\mathrm{m_{FM1}}$ in Fig. 1. Consequently, our model with consideration for the second-order frequency modulation effect provides enhanced accuracy for the frequency range around half the resonance frequency of the laser diode. It is interesting to note that there is a point where the second-harmonic distortion is greatly reduced, for example, fiber length of about 12 km in Fig. 2(b). This is due to the compensation among distortions due to different causes. The accurate prediction for this point is possible only with our model.

IV. Experimental Verification

In the above analysis, $\Delta \mathrm{I}_1(\omega)$ is used as a reference but it is not practical to experimentally measure the actual currents that are injected into the laser because of the various packaging and parasitic effects. Instead, we measured $\Delta \mathrm{P}_1(\omega)$ under the given modulation condition and use this as a reference. For the experiment, we used a commercial butterfly packaged DFB LD biased at $1.8\mathrm{I_{th}}$ and input current modulation index was set to 0.1. This is the same laser used for parameter exatraction. We measured the first-order IM response $\Delta \mathrm{P}_1$ and from that, calculated $\Delta\nu_1$ using (7). Second-order responses, $\Delta \mathrm{P}_2$ and $\Delta \mathrm{v}_2$, are determined from (9). Following above procedure, we can determine each modulation index and phase from (14). Then, we calculate second-harmonic distortion after fiber transmission, F2, from (21) and this is compared with experimentally measured second-order distortions at the given fiber length. The same procedure is repeated for several fiber length and modulation frequencies.

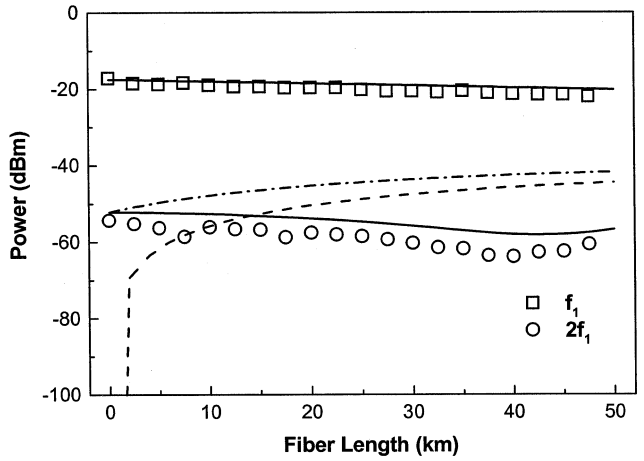

(a)

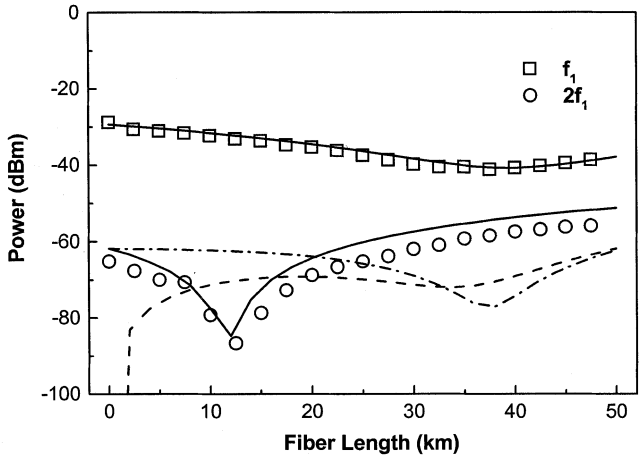

(b)

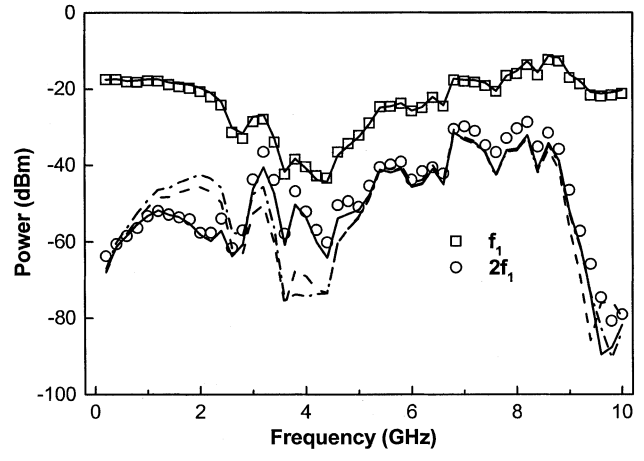

(c)

Fig. 4. Second-harmonic distortions from measurement (dots) and analyses (line) based on various models. (a) Fundamental signals and second-harmonic distortions at various fiber lengths for 2-GHz modulation. (b) Fundamental signals and second-harmonic distortions at various fiber lengths for 4-GHz modulation. (c) Fundamental signals and second-harmonic distortions at 40-km fiber for various modulation frequencies.

Fig. 3 shows the experimental setup for measuring the signal and the second-harmonic distortions at varying transmission distances. The back reflection effect is negligible because the DFB LD has a built-in isolator. In order to make sure that the measured second-harmonic distortion is due to the laser, we measured the second-harmonic nonlinearity of the modulation source, and the second-order nonlinearity of the photodetector using two optical sources modulated with different RF frequencies [13]. We confirmed they are below -70 dBc, not significant enough to influence our measurement. While compensating fiber loss with EDFA and attenuator, we measured second-harmonic distortions in the received signal by an RF spectrum analyzer.

In Fig. 4(a)–(b), results are shown that are obtained at a fixed modulation frequency of 2 and 4 GHz with varying fiber lengths. In Fig. 4(c), the results are shown for varying modulation frequencies at the fixed link length of 40 km. In the figures, dots represent measured fundamental signals and second-harmonic distortions. Calculated results with our analytical model are shown in solid lines. Good agreements with the measured results can be seen for the entire frequency ranges and transmission distances. The fluctuation in measured data in Fig. 4(c) is due to the fluctuating frequency response of the packaged DFB LD. This should not interfere with the comparison between measurement and calculation based on our model, since the calculation has taken account of the power fluctuation. For comparison, calculated results with previously reported models are also shown in dashed [5], [6] and dashed-dotted lines [7], [8], respectively. From this, we find that our model is more accurate in modeling the second-harmonic distortions in the entire frequency range and transmission distances.

V. Conclusions

We analyzed the second-harmonic distortions of the directly modulated laser diode that can be used in analog optical links. For the accurate model, intrinsic dynamics of laser diodes are considered to the second order, including the second-harmonic IM and FM indices and relative phase terms. With this, better accuracy is achieved in modeling the second-harmonic distortions for signals produced by directly modulated laser diodes and transmitted over the fiber. We confirmed the results agree well in a wide range of frequencies and transmission distances with numerically solved exact solutions as well as experimental results. We believe the results of our investigation will be useful for realizing simple analog optical links that are based on the directly modulated laser diodes.

References

[1] R. Olshansky, V. A. Lanzisera, and P. M. Hill, "Subcarrier multiplexed lightwave systems for broad-band distribution," *J. Lightwave Technol.*, vol. 7, pp. 1329–1342, Sept. 1989.

[2] T. E. Darcie and G. E. Bodeep, "Lightwave subcarrier CATV transmission systems," *IEEE Trans. Microwave Theory Tech.*, vol. 38, pp. 524–533, 1990.

[3] J. C. Fan, C. L. Lu, and L. G. Kazovsky, "Dynamic range requirements for microcellular personal communication systems using analog fiber-optic links," *IEEE Trans. Microwave Theory Tech.*, vol. 45, pp. 1390–1397, Aug. 1990.

[4] A. A. M. Saleh, "Fundamental limit on number of channels in subcarrier-multiplexed lightwave CATV system," *Electron. Lett.*, vol. 25, no. 12, pp. 776–777, 1989.

[5] G. J. Meslener, "Chromatic dispersion induced distortion of modulated monochromatic light employing direct detection," *IEEE J. Quantum Electron.*, vol. QE-20, pp. 1208–1216, Oct. 1984.

[6] C. S. Ih and W. Gu, "Fiber induced distortion in a subcarrier multiplexed lightwave system," *IEEE J. Select. Areas Commun.*, vol. 8, pp. 1296–1303, 1990.
[7] C. Y. Kuo, "Fundamental second-order nonlinear distortions in analog AM CATV transport systems based on single frequency semiconductor lasers," *J. Lightwave Technol.*, vol. 10, pp. 235–243, Feb. 1992.
[8] H. T. Lin and Y. H. Kao, "Nonlinear distortions and compensations of DFB laser diode in AM-VSB lightwave CATV applications," *J. Lightwave Technol.*, vol. 14, pp. 2567–2574, Nov. 1996.
[9] Eva Peral and Amnon Yariv, "Large-signal theory of the effect of dispersive propagation on the intensity modulation response of semiconductor lasers," *J. Lightwave Technol.*, vol. 18, pp. 84–89, Jan. 2000.
[10] J. Helms, "Intermodulation distortions of broad-band modulated laser diodes," *J. Lightwave Technol.*, vol. 10, pp. 1901–1906, Dec. 1992.
[11] J. L. Bihan and G. Yabre, "FM and IM intermodulation distortions in directly modulated single-mode semiconductor lasers," *IEEE J. Quantum Electron.*, vol. 40, pp. 899–903, Apr. 1994.
[12] L. Bjerkan and G. Yabre, "Measurement of laser parameters for simulation of high-speed fiberoptic systems," *J. Lightwave Technol.*, vol. 14, pp. 839–850, May 1996.
[13] B. Kanack, "Measurement of intermodulation distortion in optical diodes," in *IEEE MTT-S Int. Microwave Symp. Dig.*, 1995, pp. 61–64.

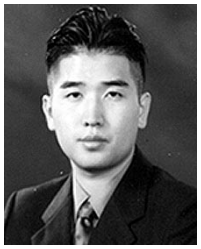

Ki-Hyuk Lee received the B.S. and M.S. degrees in electrical and electronic engineering in 2000 and 2002, respectively, from Yonsei University, Seoul, Korea, where he is currently working toward the Ph.D. degree. His Master's work involved investigating semiconductor laser-diode modeling and nonlinear distortion in analog optical links.

His research interests include microwave photonics, analog optical links and radio on fiber systems.

Hyun-Yong Choi was born in Seoul, Korea, in 1977. He received the B.S. degree (with honors) in electrical engineering from the Yonsei University, Seoul, Korea, in 2002. He is currently working toward the M.S. and Ph.D. degrees at the University of Michigan, Ann Arbor, involving research performed at the National Science Foundation Center for Ultrafast Optical Science.

His research interests include the ultrafast optical studies in semiconductor nanodevices and applications of femtosecond optical spectroscopy to semiconductor devices.

Woo-Young Choi received the B.S., M.S., and Ph.D. degrees, all in electrical engineering and computer science, from the Massachusetts Institute of Technology, Cambridge. For his Ph.D. dissertation, he investigated molecular beam epitaxy (MBE)-grown InGaAlAs laser diodes for fiber-optic applications.

From 1994 to 1995, he was a post-doctoral Research Fellow at NTT Opto-Electronics Laboratories, where he worked on femtosecond all-optical switching devices based on low-temperature-grown InGaAlAs quantum wells. In 1995, he joined the department of Electrical and Electronic Engineering, Yonsei University, Seoul, Korea, where he is presently an Associate Professor. His research interest is in the area of high-speed information processing technology, including high-speed optoelectronics, high-speed electronic circuits, and microwave photonics.